Contents list available at CBIORE journal website

International Journal of Renewable Energy Development

Journal homepage: https://ijred.cbiore.id

Research Article

Analytical computation of arm inductor for minimizing MMC circulating current using passive method

Amna Aslam and Muhammad Raza*

Department of Electrical Engineering, Bahria University, Karachi Campus, 13, National Stadium Road, Karachi 75260, Pakistan

Abstract. The study of circulating currents in modular multilevel converters is vital for improving their efficiency and reliability. The circulating current may arise from capacitor voltage unbalancing, modulation imperfections, load variations, and transient conditions. Such currents typically induce distortions in arm currents, exhibiting second-order harmonics that lead to power losses and negatively impact the ratings of converter components as well as the amplitudes of capacitor voltage ripples. Despite ongoing research, effective strategies to mitigate circulating currents are limited. This paper aims to systematically address this issue by selecting key design parameters specifically arm inductance and capacitor values, to suppress circulating currents. The methodology incorporates harmonic analysis and instantaneous power theory to derive expressions for arm inductance. Initial modelling includes common mode and differential mode analyses, leading to an examination of harmonic content. Analysis reveals that the selection of the arm inductor value is mainly influenced by the second-order harmonic component, whereas the capacitor value is determined by the fundamental harmonic component. By adopting this methodology, the boundary limit for arm inductor selection can be determined. This article proposes a novel expression for arm inductor selection. The proposed expression mainly depends on factors such as load, submodule capacitor voltages, submodule capacitor, and differential current. By selecting an appropriate inductor value based on converter-rated parameters, circulating current within the system can be effectively suppressed. The methodology offers a practical framework for arm inductor selection. Simulation results validation shows strong alignment with analytical results with the error margin of less than 1%, hereby the MMC parameter can be determined with better accuracy through analytic method.

Keywords: MMC, Converter Design, Arm Inductance, Harmonic Analysis, Arm Capacitance, Circulating Current, NLM, PSC

Received: 12th July 2024; Revised: 25th Oct 2024; Accepted: 16th Nov 2024; Available online: 4th Dec 2024

1. Introduction

Multilevel converters, widely embraced in energy and industrial systems, facilitate the design of medium voltage and high voltage systems with superior quality at the output in comparison with the two-level converters. Noteworthy advantages include simplified redundancy, reduced filter costs, and diminished losses in power semiconductors and common-mode voltages(Kouro *et al*., 2010, 2012). Multi-cell converters, characterized by high modularity, cost-effectiveness, and minimal harmonic content stand out among various topologies. Despite heightened complexity in the converter controller due to the increased number of cells, the simple structure of each cell contributes to lower manufacturing costs. Present applications include medium voltage drives, active filters, renewable energy integration, and the high-voltage direct current (HVDC) transmission systems (Malinowski *et al*., 2010; Thakur *et al*., 2022a). Modular multilevel converters (MMC), a sub-family of multi-cell converters, offer distinctive features such as transformer-less operation, a fully modular design, and a shared DC bus (Glinka & Marquardt, 2005; Yuan *et al*., 2016).

In recent years, the evolution of modular multilevel converters has witnessed substantial advancements in topology, control strategies, modulation techniques, and associated features. Despite this progress, certain critical aspects demand further attention to overcome inherent limitations and broaden the converter's application scope. Notable challenges encompass the regulation of output terminal parameters, including current, voltage, and torque, along with the charge balancing of sub modules (SMs), management of circulating current, and the mitigation of SM capacitor voltage ripple. These challenges are pivotal for ensuring the safe and dependable operation of the MMC (Camurca *et al*., 2022; Z. Liu & Zhao, 2021; Ma *et al*., 2019; Ronanki & Williamson, 2018; Spier *et al*., 2021; Tu & Xu, 2011; Vasiladiotis *et al*., 2014).Addressing these issues requires the development and deployment of high-performance control schemes, offering a strategic avenue to mitigate identified drawbacks and enhance the overall efficacy of modular multilevel converters (Fan *et al*., 2023; M. Li *et al*., 2023; Perez *et al*., 2015).

The literature (Q. Li *et al*., 2022; Reddy & Shukla, 2021) indicates that the sizing of SM capacitors in MMC is influenced by the circulating current. The voltage across SM capacitors comprises a DC component, a fundamental frequency component and higher-order harmonics with the second harmonic component being the most significant. The occurrence of second harmonic voltage component induces ripples in SM capacitor voltage, necessitating minimization or

* Corresponding author
Email: mraza.bukc@bahria.edu.pk (M.Raza)

https://doi.org/10.61435/ijred.2025.60466
ISSN: 2252-4940/© 2025.The Author(s). Published by CBIORE

suppression for ripple limitation (Li *et al.*, 2023; Lyu *et al.*, 2023; Pou *et al.*, 2015). To minimize voltage ripple in submodule (SM) capacitors and reduce their size, numerous control schemes discussed in the literature emphasize the management of the second harmonic current component. By precisely aligning this current component with specific magnitudes and phase angles, these schemes aim to suppress second harmonic voltage components within the SM capacitor arm voltages (Y. Lyu *et al.*, 2017; Picas *et al.*, 2013; Reddy & Shukla, 2019; Tu *et al.*, 2010a; Xu *et al.*, 2016). The nonlinearity of converter results in both AC and DC system producing harmonics. Recognizing the characteristics and impact of these harmonics is essential for comprehending the operation principles of MMC.

The selection of capacitor and arm inductor values is crucial in the design and development of a half-bridge modular multilevel converter (MMC). The presence of circulating current in the system significantly affects the converter's performance. One widely discussed technique in the literature for suppressing circulating current is the passive method. This technique involves the selection of an appropriate arm inductor value (Uddin *et al.*, 2018). The accurate design of MMC circuit parameters necessitates extensive calculations, underscoring the importance of developing an analytical model for the harmonic characteristics of MMCs as previously investigated by others (Liu *et al.*, 2019; Sang *et al.*, 2019; Zhang *et al.*, 2021). Such a model is crucial for both theoretical insights and practical design applications, as noted by (Kumar *et al.*, 2019; Song *et al.*, 2013; Xiao *et al.*, 2013; Yuvaraja & Mazumder, n.d.).

The expressions derived in some articles (Tu *et al.*, 2010b; Xu *et al.*, 2016) contain assumptions that neglect higher-order harmonics. The novelty of this work lies in deriving an arm inductor expression that considers all components present in the system. Then harmonic addition theorem is applied to sine and cosine terms of power at double fundamental frequency. By incorporating harmonic analysis and instantaneous power theory, arm inductor expression has been derived. This article provides a detailed model for a half-bridge submodule based multilevel converter. It shows the mathematical formulation and explains the determination of arm inductor values and their impact on circulating current. Following this, a modulation technique is applied to extract the harmonic information inherent in the system. Fourier analysis is then used as the primary analytical tool, facilitating a detailed evaluation of the harmonic components. The resulting harmonic dynamics are analytically ascertained and validated against an implemented system using MATLAB/Simulink/ PLEXIM. The systematic approach proposed here not only covers the intricacies of implementing the half-bridge MMC design but also offers insights into its harmonic characteristics.

2. Modelling and Control of MMC

In MMC, the half-bridge sub-module (HBSM) configuration involves the connection of multiple sub-modules in series to form one arm. Each phase comprises of upper arm and lower arm that collectively form phase leg. These sub-modules functioning as a complementary mode switch, comprises a pair of MOSFETs along with a filter capacitor (Raza *et al.*, 2023). To regulate current, an inductor is incorporated in each arm. The systematic activation and deactivation of switching states enable a progressive, incremental development of the output voltage with N sub modules present in each arm.

The structural arrangement of a phase leg in the MMC along with equivalent models are illustrated in Fig. 1. A common mode and differential mode equivalent models of MMC can be developed to examine the converter behaviour and harmonics

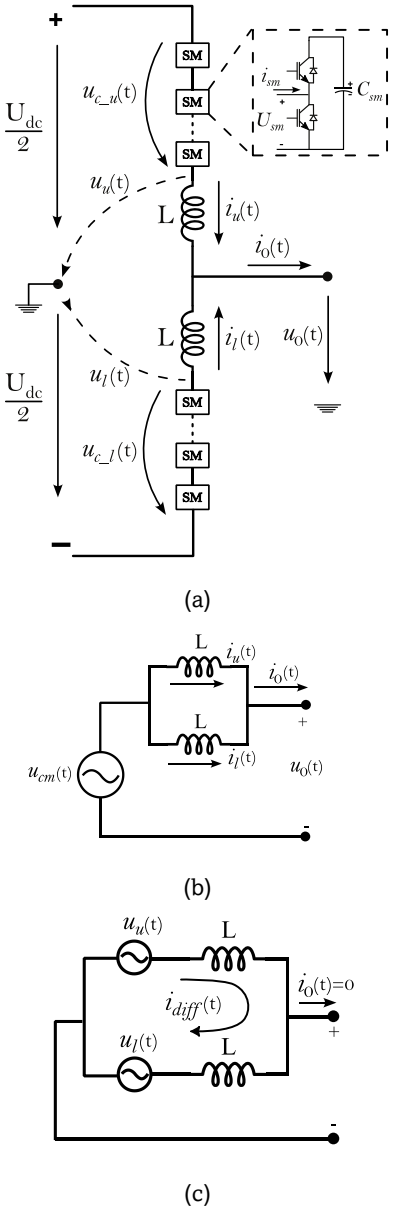

Fig. 1 (a) Single phase MMC configuration, (b) Common mode equivalent (c) Differential mode equivalent model

analyse based on instantaneous theory (Ji-Woo Moon *et al.*, 2013; S. Li *et al.*, 2015; Thakur *et al.*, 2022b; Wang *et al.*, 2016; B. Zhang & Nademi, 2020). In the common mode, the current $i_0(t)$ flows from the supply line to the load, combining the upper and lower arm currents. On the other hand, in the differential mode, the current $i_{diff}(t)$ circulates with in the converter. The circulating current is not reflected in the load current rather circulate in the arms. The circulating current appears due to imbalance between inductor values, and the voltage difference between the upper and lower arms.

The voltage across upper and lower arms SMs, $u_{c_u}(t)$and $u_{c\_l}(t)$ respectively, can be represented as equivalent voltage sources generated through switching patterns. Considering the fictitious DC bus midpoint as the reference or 0, the voltage provided by the upper and lower arms, $u_u(t)$ and $u_l(t)$ respectively, can be defined as (1) and (2).

$$u_u(t) = \frac{U_{dc}}{2} - u_{c\_u}(t) \quad (1)$$

$$u_l(t) = -\frac{U_{dc}}{2} + u_{c\_l}(t) \quad (2)$$

The phase voltage or output voltage is designated by $u_0(t)$, thus using KVL upper and lower closed loop differential equation can by derived (3) and (4).

$$u_u(t) = L\frac{di_u(t)}{dt} + u_0(t) \quad (3)$$

$$u_l(t) = L\frac{di_l(t)}{dt} + u_0(t) \quad (4)$$

Where, $i_u(t)$ and $i_l(t)$ are the upper and lower arms current respectively. It is assumed that both arm inductors have same value. The output voltage equation can be derived as (5)

$$u_0(t) = \frac{u_u(t) + u_l(t)}{2} - L\frac{d}{dt}\left(\frac{i_u(t) + i_l(t)}{2}\right) \quad (5)$$

In (5), the first term in the right-hand side is the common mode voltage and the second term is the voltage drop across inductors. The current at the output is basically the sum of upper arm current and lower arm current as defined by (6).

$$u_L(t) = \frac{L}{2}\frac{di_0(t)}{dt}$$
$$i_0(t) = i_u(t) + i_l(t) \quad (6)$$

Application of KVL on differential mode equivalent circuit gives the relationship between differential voltage $u_{diff}(t)$ and current $i_{diff}(t)$ as defined in (7) and (8). A differential current would be in phase with $i_u(t)$ but opposite in direction of $i_l(t)$ considering the same sign convention as in common mode.

$$u_u(t) - u_l(t) = L\frac{d}{dt}\left(i_u(t) - i_l(t)\right) \quad (7)$$

$$u_u(t) - u_l(t) = L\frac{di_{diff}(t)}{dt} + L\frac{di_{diff}(t)}{dt}$$

$$u_{diff}(t) = L\frac{di_{diff}(t)}{dt} \quad (8)$$

$$u_{diff}(t) = \frac{1}{2}\left(u_u(t) - u_l(t)\right)$$

Differential current would not flow through the load rather circulates in the arm. Differential current generates the same voltage drops across both inductors considering no parametric variation. The differential current in term of upper and lower arm current can be written as (9). It is obvious from (7) that the differential current appears due to difference in upper and lower arm voltages. The main cause for this difference is the unbalance in SM capacitor voltages and non-ideal switching pattern.

$$i_{diff}(t) = \frac{1}{2}\left(i_u(t) - i_l(t)\right) \quad (9)$$

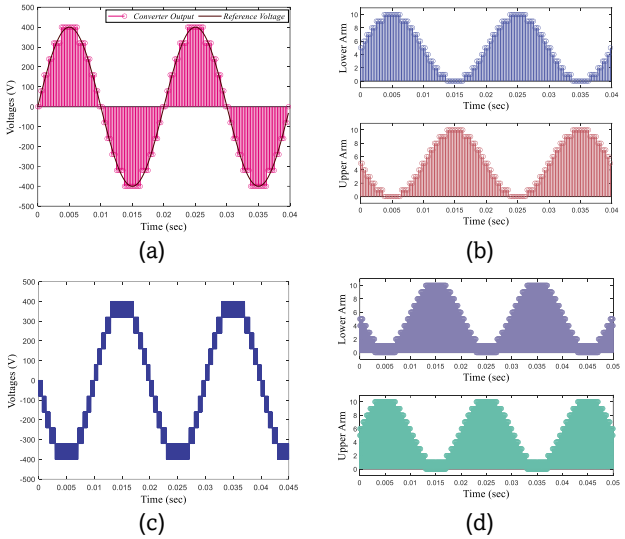

Fig. 2 (a) Output voltage using NLM (b) Switching operations of the upper and lower arms SMs using NLM (c) Output voltage using PSC (d) Switching operations of both arms SMs using PSC

Both load and differential current flows in upper and lower arms as defined by (10). Similarly, the total voltage drop across inductors would also be due to both load and differential current.

$$i_u(t) = \frac{i_0(t)}{2} + i_{diff}(t)$$
$$i_l(t) = \frac{i_0(t)}{2} - i_{diff}(t) \quad (10)$$

3. Analytical Calculation for the MMC Arms Inductance

The analytical determination of the arm inductance in MMC is feasible. It establishes a correlation between the arm inductance and the second order circulating current, offering a criterion for selecting the appropriate arm inductance in accordance with the circulating current limit.

The proposed methodology to determine the inductor value for the half bridge modular multilevel converter is validated through dynamic simulation performed in MATLAB/SIMULINK and PLEXIM. The network parameters are given in Table 1. For system analysis, a switching model of SMs is implemented. A 5kVA converter is modeled for analysis with the DC link voltages set to 800V. The design includes 10 sub-modules in both the upper and lower arms. Based on the expressions stated above, each sub-module (SM) capacitor has a capacitance of 4700μF, with an SM capacitor voltage of 80V. A load of 4.840 kW is connected to the system for this analysis.

3.1 Harmonic Analysis of MMC Voltage and Current

In MMC, low voltage power semi-conductor switches are serially interconnected to attain higher voltage output. The control of individual SMs arm voltage is pivotal. The switching pattern of these switches depends on the modulation techniques, two prominent modulation techniques employed

Table 1
Parameters for system analysis

Parameters	Values
Peak Voltages (V)	400.0
Per SM Capacitance (μF)	4700.0
Per SM Voltage (V)	80.0
Rated Power (kVA)	5.0
Angular Frequency (rad/s)	314.0
Energy Power Ratio (J/kVA)	60.0
Nominal Frequency (Hz)	50.0
Switching Frequency (kHz)	2.0
DC Bus Voltage (V)	800.0
Number of SMs per Phase	20.0
Modulation Index	1.0

are NLM and PSC. These techniques help in shaping the output waveform and to meet design requirements with in the MMC framework (António-Ferreira *et al.*, 2018; Ilves *et al.*, 2015; Nguyen & Kwak, 2021; C. Xu *et al.*, 2020). The sampling frequency in modulation is responsible for generating a discrete signal by taking a number of samples from a continuous signal in unit time. The crucial factor is the minimum sampling time Ts, determined by using (11).

$$\Delta T_s = \frac{1}{\omega}\, sin^{-1}(\frac{4}{N \cdot M}) \tag{11}$$

where ω is the angular frequency N is the number of SMs and M is the modulation index. It is important to uphold a modulation index within the range of 0.7 to 1.0. The sampling period Ts is crucial for maintaining a smooth generation of output voltage, ensuring that all voltage levels are captured without omission. In Fig. 2, graphical representations of both output waveforms and switching operations for both the NLM and PSC are provided. In the NLM, the accurate sampling frequency facilitates the formation of the nearest voltage level. While in the PSC, precise selection of sampling and switching frequencies enables the creation of a staircase waveform without any voltage gaps.

Both the NLM and PSC showcase the presence of a DC component, fundamental component, and various even and odd harmonics across both the upper and lower arms. Notably, the even harmonics share identical magnitude and phase angles, leading to their mutual cancellation, while the odd harmonics maintain the same magnitude but undergo a180-degree phase shift.

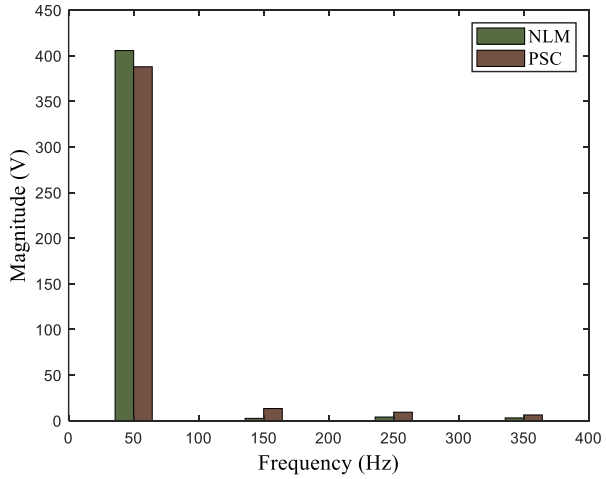

Fig. 3 Output voltages FFT analysis for both NLM and PSC

$$\begin{aligned} u_{c\_l}(t) = \frac{U_{dc}}{2} &+ U_p\, sin(\omega t + \delta) \\ &+ U_{3p}\, sin(3\omega t + \delta_3) \\ &+ U_{5p}\, sin(5\omega t + \delta_5) \\ &+ U_{7p}\, sin(7\omega t + \delta_7) + \cdots \\ u_{c\_u}(t) = \frac{U_{dc}}{2} &- U_p\, sin(\omega t + \delta) \\ &- U_{3p}\, sin(3\omega t + \delta_3) \\ &- U_{5p}\, sin(5\omega t + \delta_5) \\ &- U_{7p}\, sin(7\omega t + \delta_7) - \cdots \end{aligned} \tag{12}$$

The Fourier analysis depicted in Fig. 3 highlights the overall response, emphasizing the presence of the fundamental component and odd harmonics. The acquired harmonic information serves as the foundation for formulating other harmonics for load currents and voltages as (13) and (14). The common mode current $i_0(t)$ consists of a fundamental component, odd harmonics, and an initial transient dc component. The transient dc component decays over time, leaving behind the primary fundamental part and odd harmonics in the system.

$$\begin{aligned} u_o(t) = U_p\, cos(\omega t + \delta) &+ U_{3p} \cos(3\omega t + \delta_3) \\ &+ U_{5p} \cos(5\omega t + \delta_5) + \cdots \end{aligned} \tag{13}$$

$$\begin{aligned} i_o(t) = I_p\, cos(\omega t + \psi) &+ I_{3p}\, cos(3\omega t + \psi_3) \\ &+ I_{5p}\, cos(5\omega t + \psi_5) + \cdots \end{aligned} \tag{14}$$

Upon the substitution of $u_{c\_u}(t)$ and $u_{c\_l}(t)$ in equation (1) and (2) respectively, the harmonic content of $u_u(t)$ and $u_l(t)$ becomes evident. By using (8) the harmonic characteristics of $u_{diff}(t)$ and $i_{diff}(t)$ were determined. The $u_{diff}(t)$ encompasses exclusively even harmonics, while $i_{diff}(t)$ comprises both DC components and even harmonics. The initial values of the DC component are derived from (Pou *et al.*, 2015), allowing the formulation of the equation for $i_{diff}(t)$ as presented in (15).

$$\begin{aligned} i_{diff}(t) = I_{dc} &+ I_{2p}\, cos(2\omega t + \psi_2) \\ &+ I_{4p}\, cos(4\omega t + \psi_4) + \cdots \end{aligned} \tag{15}$$

Substitute $i_{diff}(t)$ in (10), so upper arm current $i_u(t)$and lower arm current $i_l(t)$ can be expressed as (16):

$$\begin{aligned} i_u(t) = I_{dc} &+ I_{pu}\, cos(\omega t + \psi) \\ &+ I_{2pu}\, cos(2\omega t + \psi_2) \\ &+ I_{3pu}\, cos(3\omega t + \psi_3) \\ &+ I_{4pu}\, cos(4\omega t + \psi_4) + \cdots \\ i_l(t) = I_{dc} + I_{pl}\, cos(\omega t + \psi) &+ I_{2pl}\, cos(2\omega t + \psi_2) \\ &+ I_{3pl}\, cos(3\omega t + \psi_3) \\ &+ I_{4pl}\, cos(4\omega t + \psi_4) + \cdots \end{aligned} \tag{16}$$

3.2 Sub-Module Capacitor Power and Energy Dynamics

Instantaneous power across the arm capacitors:

$$\begin{aligned} p_{cu}(t) &= u_{c\_u}(t)\, i_u(t) \\ p_{cl}(t) &= u_{c\_l}(t)\, i_l(t) \end{aligned} \tag{17}$$

After substitution, the power in upper and lower arm will be expressed as:

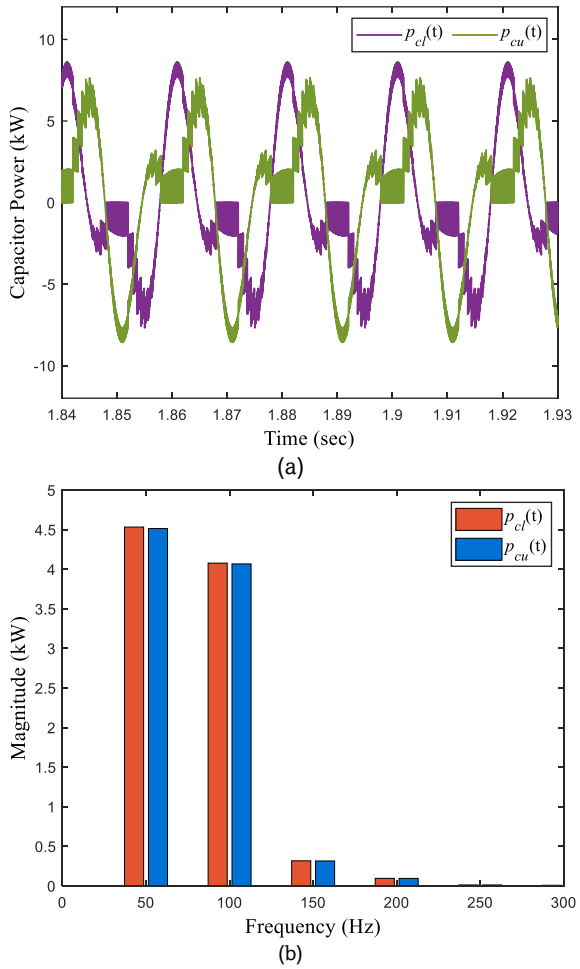

Fig. 4 Arms Capacitor Power (a) Instantaneous Response (b) Fourier Analysis

$$p_{cu}(t) = \left(\frac{U_{dc}}{2} - u_o(t) - u_L(t)\right) \cdot \left(\frac{i_o(t)}{2} + i_{diff}(t)\right)$$
$$p_{cl}(t) = \left(\frac{U_{dc}}{2} + u_o(t) + u_L(t)\right) \cdot \left(\frac{i_o(t)}{2} - i_{diff}(t)\right) \quad (18)$$

In accordance with the sign convention the net power and the difference in power for both upper and lower arms across the capacitor can be written as:

$$\Sigma p_c = \frac{U_{dc}\, i_o(t)}{2} - 2u_o(t)\, i_{diff}(t) - 2u_L(t)\, i_{diff}(t)$$
$$\Delta p_c = U_{dc}\, i_{diff}(t) - u_o(t) i_o(t) - u_L(t) i_o(t) \quad (19)$$

Equation (19) illustrates the summation of the upper and lower arm capacitor powers, as well as the difference between their powers. The Σp_c component arises from the common mode, whereas Δp_c originates from the differential mode. Both the cumulative and differential arm powers represent the capacitor power in the system. Terms denoted with a positive sign denote power supplied by the source, whereas those with negative sign signify the load consumption.

Previous harmonic analysis has provided insights into the harmonic characteristics within the power profiles of both upper and lower arms. These components include a fundamental component as well as a combination of even and odd harmonics, as depicted in Fig. 4. Fig. 4(a) illustrates the output waveform of capacitors in both upper and lower power arms over time. The presence of harmonics in the system is evident from the distortion observed in the waveform. Furthermore, Fig. 4(b) presents the Fourier analysis of capacitor power, revealing the significant presence of the fundamental component and the dominance of the second harmonics. The preceding expressions highlight the prevalence of sine and cosine terms in the total power within the system. The magnitude of its double fundamental frequency component is notably high compared to other even harmonics so leads to the formulation of (20).

$$\begin{aligned} p_{2\omega}(t) = \frac{1}{\omega^3 L^3 + 4\omega L R^2} \\ \cdot \big[\, 0.5\, U_{dc} L^2 \omega^2 U_{2p} \cos(2\omega t + \phi_2) \\ + \, 2\, U_{dc}\, R^2 U_{2p} \cos(2\omega t + \phi_2) \\ + 2\, U_p^2\, LR\omega \cos(2\omega t + \phi_2) \\ - \, 4\, U_{2p}^2\, R^2 sin(2\omega t + \phi_2) \\ + \, Up^2 L^2 \omega^2 sin(2\omega t + \phi_2) \\ - \, U_{2p}^2\, L^2 \omega^2 sin(2\omega t + \phi_2) \\ + \, 8\, U_{2p}\, I_{dc}\, LR^2 \omega \sin(2\omega t + \phi_2) \\ + 2\, U_{2p}\, I_{dc}\, L^3\, \omega^3 sin(2\omega t + \phi_2)\, \big] \end{aligned} \quad (20)$$

From the analysis of total power, attention is directed towards dominant sine and cosine terms. These terms collectively form the primary double fundamental frequency component, crucial for generating second harmonics within the system. In the equation (20), the third and fifth term were identified as prominent contributors to the double frequency components. The harmonics addition theorem is then applied to express the sum of sinusoidal functions in a unified single sinusoid form, as shown in (21)

$$p_{2\omega}(t) = \frac{U_p^2}{\sqrt{\omega^2 L^2 + 4R^2}} \cdot cos(2\omega t + \phi_2) \quad (21)$$

The total stored energy across the capacitors can be written as:

$$W_c(t) = N \cdot \frac{1}{2}\, C_{sm}\, u_c^2(t) \quad (22)$$

Both the upper and lower arms capacitor voltages consist of fundamental components and other harmonics. But the total capacitor voltage in a leg is characterized by the presence of a DC component and a second harmonic component. $u_c(t)$ signifies the total capacitor voltages within a leg and defined as:

$$u_c(t) = U_{sm} + \frac{2}{N}\left(U_{2p} \sin(2\omega t + \delta_2)\right) \quad (23)$$

Upon substituting uc(t) and subsequently taking the derivative of Wc(t), the power expression is derived as (24)

$$\begin{aligned} \frac{dW_c(t)}{dt} = 4\omega C_{sm} U_{sm} U_{2p} \cos(2\omega t + \phi_2) \\ + \frac{4C_{sm}\omega U_{2p}^2}{N} \cdot sin(4\omega t + \phi_4) \\ + \cdots \end{aligned} \quad (24)$$

Comparing (21) and (24), the components at double fundamental frequency be equal to:

$$4\omega C_{sm} U_{sm} U_{2p} = \frac{U_p^2}{\sqrt{\omega^2 L^2 + 4R^2}} \quad (25)$$

The voltage at double fundamental frequency U2p is determined as:

$$U_{2p} = \frac{U_p^2}{4\omega C_{sm} U_{sm} \cdot \sqrt{\omega^2 L^2 + 4R^2}} \quad (26)$$

The current I2p Gat double fundamental frequency can be calculated as:

$$I_{2p} = \frac{U_{2p}}{2\omega L} \quad (27)$$

Upon substituting U_{2p} into (27), I2p becomes:

$$I_{2p} = \frac{U_p^2}{8\omega^2 L C_{sm} U_{sm} \cdot \sqrt{\omega^2 L^2 + 4R^2}} \quad (28)$$

By using these equations, a comprehensive formulation for inductor L has been derived as (29)

$$L = \frac{\sqrt{2}R}{\omega} \cdot \sqrt{\left\{\left(\frac{I_p^2}{16\omega C_{sm} U_{sm} I_{2p}}\right)^2 + 1\right\}^{1/2} - 1} \quad (29)$$

The value of L, as indicated in (29) in Henry, relies on the load current (I_p), the submodule capacitor voltage (U_{sm}), and submodule capacitor (C_{sm}). C_{sm} values were chosen based on the converter rated power, submodule count, DC voltages and energy power ratio (EP), denoting the ratio of maximum stored energy and the rated power. Typically, EP ranges from 10J/kVA to 80J/kVA in converter applications, impacting cost and voltage ripple. A lower EP reduces converter cost but increases voltage ripple.

4. Analytical Results and Discussion

For the simulation, a direct modulation method is applied to the MMC network depicted in Figure 1(a). Direct modulation refers to a control technique in which the reference signals directly modulated in converter's upper and lower arms to control the submodules' switching states. It does not include circulating current control which leads to high circulating current and capacitor voltage ripples. Therefore, circulating current can only be limited by selecting appropriate inductor values to keep the circulating current within the limits (Lizana *et al.*, 2015; Nguyen & Kwak, 2020). It is not possible to eliminate the circulating current completely using only passive method rather it can only be reduced. Therefore, inductor value is determined through analytical method in the proposed research to achieve the desired circulating current magnitude. In the presented research, arm inductor value is calculated using (29) whereas the circulating current value can be determined using (28). It is clear from the equations that these values depend on the load current, SM voltages, and output voltage.

The analysis of I2p and U2p with respect to arm inductor value is shown in Figure 5. The response shows the comparison between the analytical and simulated results. The analytical calculation showing a close alignment with the simulation results for the value above 10mH. Through response of Figure 5, the required value of inductor can be determined according to the desired circulating current magnitude. The magnitude of the differential current decreases as inductor values increases. However, higher value of inductor cannot be selected due to the voltage drop across it at fundamental frequency thus inductor value between 20mH to 35mH is suitable. At 50mH and 50Hz, the reactance value is 15.7Ω which would cause the voltage drop of 74V across it at full load. Low inductor values require large capacitors which are impractical for design. On the other hand, high inductor values cause significant voltage drops affecting voltage regulation. Therefore, maintaining the inductance within the 20 to 35mH range is suitable for achieving a stable and robust system.

According to the designed criteria, the 30mH inductor value is suitable which would limit the circulating current magnitude to 0.825A at full load with voltage drop of 26V. The proposed arm inductor value gives better results as compared to other's research. Such as, the derived expression in the article by (Tu *et al.*, 2010b) excludes current and voltage higher-order harmonics which compromises the accuracy of the results. Based on the parameter of (Tu *et al.*, 2010b), the I2p values is 951.65A for single phase MMC with 40MW and ±20kV. While the proposed equation provides more optimized value of inductor which leads to the reduction of circulating current up to 303.72A. Similarly, in article (X. Li *et al.*, 2016) experimental results are given for the system of 10kVA with 625V DC. The results given I2p value of 2.18A using 12mH arm inductance. The same designed parameters have been used to validate the proposed arm inductor equation. The expression gives inductor value of 10mH which is closed to practically used value. Thus, this demonstrates that including all harmonics results in a more accurate selection of components. Whereas the non-linear behaviour of U2p remains within an acceptable deviation, as it is influenced by additional factors. Specifically, between 25mH to 35mH, the error margin for U2p remains below 1V, with both

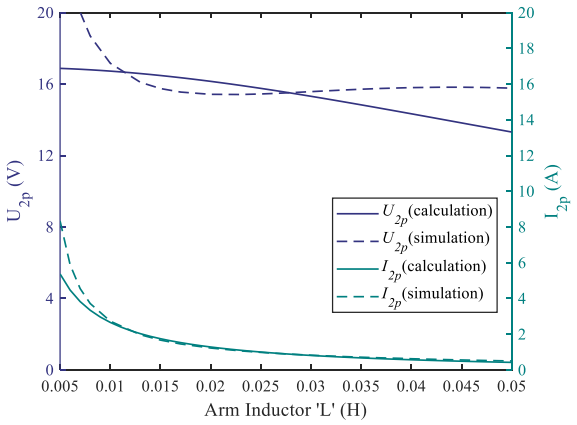

Fig. 5 Results of differential voltage (U_{2p}) and current (I_{2p}) at different values of arm inductor (L)

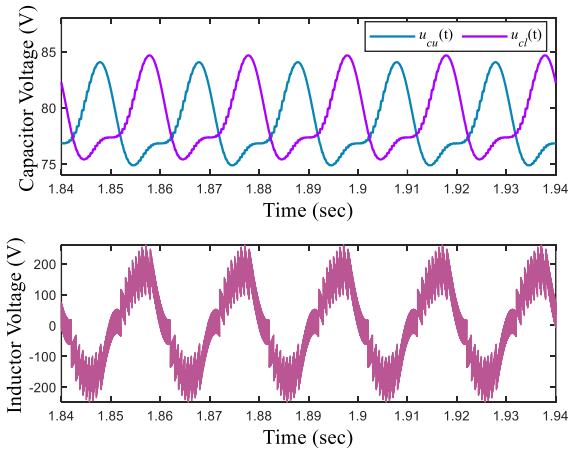

Fig. 6. Capacitor and inductor voltages response at 30mH

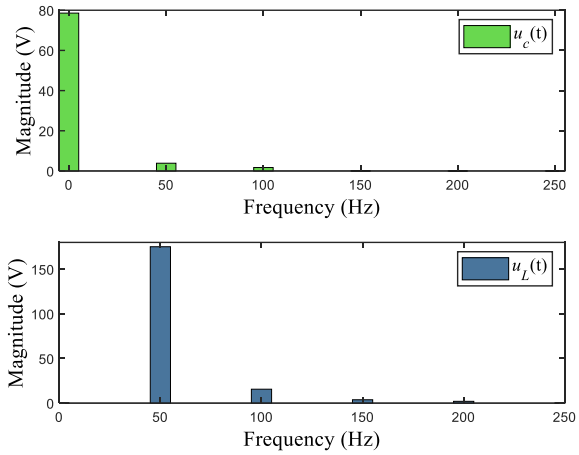

Fig. 7 Capacitor Voltage of a SM, and voltage of an arm inductor FFT Response at 30mH.

simulated and calculated values fluctuating between 15V and 16V.

The output waveform of capacitor voltage and inductor voltages is shown in Figure 6. It is clear from the results that the capacitor voltage contains both DC voltage and voltage ripples. The DC voltage indicates the stored energy whereas the voltage ripples are due to the system harmonics. The harmonic profile of the capacitor voltage is shown in Figure 7. The harmonic profile shows that each capacitor voltage contains 50Hz component with magnitude of 3.85V while 1.7V at 100Hz. All the 20 SMs of the MMC-converter shows the same voltage profile. The harmonics in the capacitor voltage appears due to circulating current. The circulating current affects the capacitor voltages and causes energy to flow back and forth between the capacitor and the inductor. Therefore, the submodules should be sized to withstand these ripples. It can be observed from Figure 6 that the peak-to-peak capacitor voltages is 10V. At the lower inductor value, peak-to-peak ripple voltages increases. The nature of the capacitor voltage waveforms is like that reported in the article (He *et al.*, 2015; Xi *et al.*, 2024), confirming that the findings are consistent across different approaches. In article (He *et al.*, 2015), the second harmonic component in the capacitor voltage is reduced up to 6V using a PI controller while wit h optimum selection of the inductor value using proposed expression leads to lower harmonics voltage i.e., 3V. Passive method would be sufficient for certain case, low to medium power rating system, to reduce the second harmonic component consequently reduces the control complexity.

The time domain response of an inductor voltage shows that high frequency harmonics are also presented. These harmonics are due to switching frequency. In the research, PSC modulation technique is applied for the SM simulation with the switching frequency of 2kHz. The high-frequency harmonics occur at the switching frequency along with its multiples i.e., 4 kHz, 8 kHz etc. Furthermore, sub-harmonics of switching frequency are also present and have higher magnitude than switching harmonics (Ren *et al.*, 2021). The magnitude of harmonics at a switching frequency of 2kHz is 0.2V, whereas the dominant sub-harmonics at 2kHz frequency have a magnitude of 13V. Similarly, the harmonic magnitude at 4kHz of inductor voltage is 0.0765V while its sub-harmonics maximum voltage is 5.4V. The upper and lower arm inductor voltage odd harmonics are in phase while even harmonics are 180° phase shifted from each other. Thus, the upper and lower arm even harmonics are

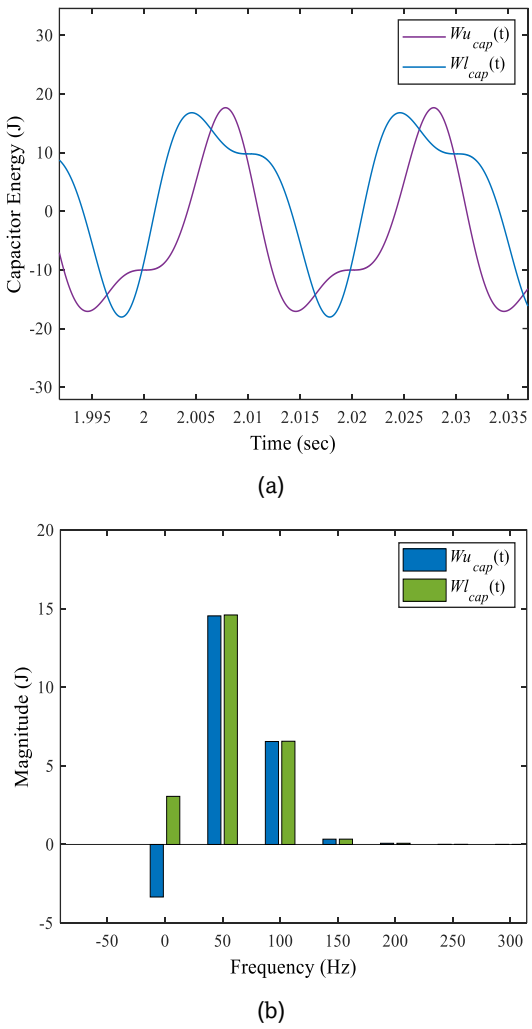

Fig. 8 Capacitor Arm Energy (a) Waveform of Upper and Lower Arm (b) Harmonic Response at 30mH

cancelled in common mode and does not appear in the output voltage. On the other hand, odd harmonics appears in the output voltage. The odd harmonics in the arm inductor are lower than even harmonics which is evident from the Figure 7 i.e., 175.5V at 50Hz, 16V at 100Hz, and 3.8V at 150Hz. Also, the magnitude of switching frequency harmonics is lower than 100Hz component. Thus, harmonic filter is not required to be designed for switching frequency. Since, 100Hz component is predominate in inductor voltage, inductor sizing based on circulating current (i.e., 100Hz) would be sufficient to filter out the harmonics. Reduction in the inductor voltage even harmonics consequently reduces the 100Hz component in the capacitor voltage hereby reduces the ripples.

The capacitor energy waveforms in the upper and lower arms exhibit a dynamic oscillating behavior as shown in Figure 8. These oscillations are due to the flow of AC current, which periodically charges and discharges each arm's capacitors. The variation of capacitor energy in MMC arms results in capacitor voltage fluctuations. The nature of capacitor energy is similar as reported in article (Hafeez *et al.*, 2020). From Figure 8(a), the capacitor energy in both the upper and lower arms oscillates between approximately +18J and −18J. This indicates a peak-to-peak energy variation of 36J. The energy waveforms observed in both the upper and lower arms exhibit

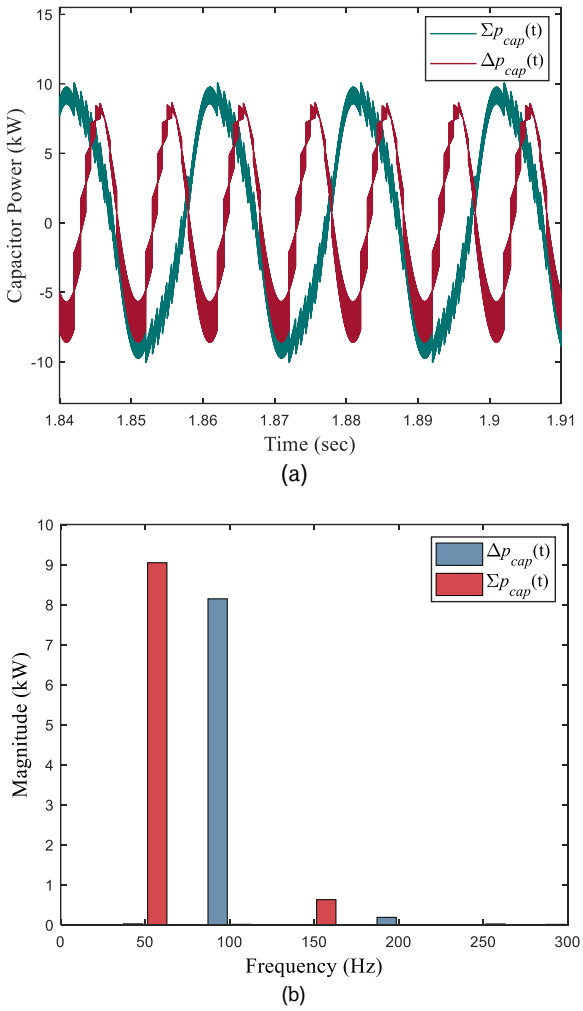

Fig. 9 Composite analysis of capacitor power in upper and lower arms

oscillations centered around a non-zero average showing the presence of DC component. Furthermore, the sinusoidal pattern of these energy curves shows the fundamental frequency components, along with the low-order harmonics. Fig 8(b) shows the harmonic response of capacitor upper and lower arm energy. The magnitude of upper arm DC stored energy is -3.34J while the magnitude of lower arm DC stored energy is 3.0612J. This reflects the roles of each arm during the charging and discharging processes in converter operation. Whereas the magnitude of fundamental component in both arms is 14.6J. The magnitude at 100Hz and 150 Hz are approximately same i.e., 6.55J and 0.339J respectively for both upper and lower arms.

The harmonics in the SMs voltage can be understood through its net power and energy store in it. The instantaneous power of SMs in common and differential mode are shown in Fig 9(a). The common mode power contains the odd harmonics whereas in differential mode even harmonics are present as shown in Fig 9(b). It is obvious that the DC power supply by the DC source is equal to the active power of the AC load thus no DC component would appear in the capacitor power. The dominate harmonics in the capacitor power is 50Hz with magnitude of 9.04kW consequently the 50Hz component is dominate in the SMs capacitor voltage ripple. On the other hand, the magnitude of double fundamental frequency

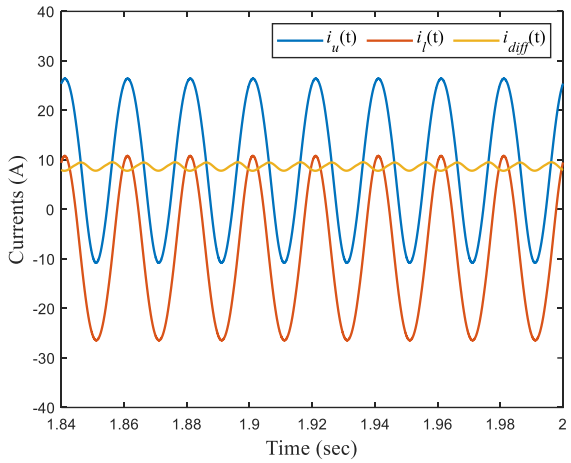

Fig.10 Instantaneous Current Response of (a) Upper Arm (b) Lower Arm (c) Differential Current.

component is 8.14 kW whereas the magnitude of fourth order harmonic component is 0.188 kW. It is clear that fundamental and second order harmonics are significant in the capacitor power and voltages.

The half-bridge MMC model configured with a 30mH inductor and a 4700μF capacitor per SM, resulting in sinusoidal waveforms for both the upper arm current and the lower arm current. These waveforms exhibit a noticeable DC offset. This offset indicates a shift from the zero-current reference line and reflects the energy balance maintained within the converter. The differential current illustrated in the Figure 10 is derived from the average of the currents in upper arm and lower arm (Hafeez *et al.*, 2019). This relationship highlights the contributions of both arms to overall stability. The lower arm current and upper arm current have a peak-to-peak value of approximately 38A. The magnitude of the DC offset is 8.7A and the magnitude of I2p is 0.9A. The sinusoidal nature of the waveforms and the observed DC offsets indicate that the analytically derived expression for the arm inductor effectively ensures system stability.

6. Conclusion

In conclusion, this study has demonstrated the importance of common and differential mode analysis in the modeling of modular multilevel converter. An analytical approach has been employed for the selection of the arm inductor. This approach uses mathematical model based on harmonic analysis and the dynamics of power and energy within sub-modules. By focusing on dominant terms such as sine and cosine, an expression for arm inductor selection has been derived. This expression exhibits enhanced accuracy compared to other literature in which there is an error margin of approximately 5%. In contrast, the derived expression presents an error margin of less than 1%. A simulation-based model has been implemented incorporating these modeling equations and NLM and PSC modulation techniques. The study concludes within the specified range of 25mH to 35mH the I2p error margins remain below 1% and the U2p error is notably low. The paper presents a thorough analysis of the system's components, deriving mathematical expressions and conducting harmonic analysis to assess the system's response. As a result, the validity of the arm inductor

expression is confirmed, demonstrating its reliability for practical applications.

Author Contributions: All authors have read and agreed to the published version of the manuscript and contributed equally.

Funding: This research is funded by Higher Education Commission of Pakistan under National Research Program for University (NRPU-14579).

Conflicts of Interest: The authors declare no conflict of interest.

References

António-Ferreira, A., Collados-Rodríguez, C., & Gomis-Bellmunt, O. (2018). Modulation techniques applied to medium voltage modular multilevel converters for renewable energy integration: A review. *Electric Power Systems Research*, *155*, 21–39. https://doi.org/10.1016/j.epsr.2017.08.015

Camurca, L., Pereira, T., Hoffmann, F., & Liserre, M. (2022). Analysis, Limitations, and Opportunities of Modular Multilevel Converter-Based Architectures in Fast Charging Stations Infrastructures. *IEEE Transactions on Power Electronics*, *37*(9), 10747–10760. https://doi.org/10.1109/TPEL.2022.3167625

Fan, Z., Wan, Z., Gao, L., Xiong, Y., & Song, G. (2023). A Multi-Objective Optimal Configuration Method for Microgrids Considering Zero-Carbon Operation. *IEEE Access*, *11*, 87366–87379. https://doi.org/10.1109/ACCESS.2023.3303926

Glinka, M., & Marquardt, R. (2005). A New AC/AC Multilevel Converter Family. *IEEE Transactions on Industrial Electronics*, *52*(3), 662–669. https://doi.org/10.1109/TIE.2005.843973

Hafeez, K., Khan, S. A., Van den Bossche, A., & Eddinne, K. D. (2020). Capacitor Energy Variations in MMC Using Harmonics Injection. *Power Electronics and Drives*, *5*(1), 97–107. https://doi.org/10.2478/pead-2020-0007

Hafeez, K., Khan, S. A., Van den Bossche, A., & Hasan, Q. U. (2019). Circulating Current Reduction in MMC-HVDC System Using Average Model. *Applied Sciences*, *9*(7), 1383. https://doi.org/10.3390/app9071383

He, L., Zhang, K., Xiong, J., & Fan, S. (2015). A Repetitive Control Scheme for Harmonic Suppression of Circulating Current in Modular Multilevel Converters. *IEEE Transactions on Power Electronics*, *30*(1), 471–481. https://doi.org/10.1109/TPEL.2014.2304978

Ilves, K., Harnefors, L., Norrga, S., & Nee, H. P. (2015). Analysis and operation of modular multilevel converters with phase-shifted carrier PWM. *IEEE Transactions on Power Electronics*, *30*(1), 268–283. https://doi.org/10.1109/TPEL.2014.2321049

Kouro, S., Malinowski, M., Gopakumar, K., Pou, J., Franquelo, L. G., Bin Wu, Rodriguez, J., Pérez, M. A., & Leon, J. I. (2010). Recent Advances and Industrial Applications of Multilevel Converters. *IEEE Transactions on Industrial Electronics*, *57*(8), 2553–2580. https://doi.org/10.1109/TIE.2010.2049719

Kouro, S., Rodriguez, J., Wu, B., Bernet, S., & Perez, M. (2012). Powering the Future of Industry: High-Power Adjustable Speed Drive Topologies. *IEEE Industry Applications Magazine*, *18*(4), 26–39. https://doi.org/10.1109/MIAS.2012.2192231

Kumar, A. R., Bhaskar, M. S., Subramaniam, U., Almakhles, D., Padmanaban, S., & Bo-Holm Nielsen, J. (2019). An Improved Harmonics Mitigation Scheme for a Modular Multilevel Converter. *IEEE Access*, *7*, 147244–147255. https://doi.org/10.1109/ACCESS.2019.2946617

Li, M., Dong, N., Chang, X., Yang, H., & Zhao, R. (2023). Analysis and Suppression of Capacitor Voltage Ripple for Hybrid MMCs under Boosted AC Voltage Conditions. *IEEE Journal of Emerging and Selected Topics in Power Electronics*, *11*(4), 3775–3787. https://doi.org/10.1109/JESTPE.2023.3268847

Li, Q., Li, B., He, J., Prieto-Araujo, E., Westerman Spier, D., Lyu, H., & Gomis-Bellmunt, O. (2022). A novel design of circulating current control target to minimize SM capacitance in MMC. *International Journal of Electrical Power & Energy Systems*, *143*, 108432. https://doi.org/10.1016/j.ijepes.2022.108432

Li, S., Wang, X., Yao, Z., Li, T., & Peng, Z. (2015). Circulating Current Suppressing Strategy for MMC-HVDC Based on Nonideal Proportional Resonant Controllers Under Unbalanced Grid Conditions. *IEEE Transactions on Power Electronics*, *30*(1), 387–397. https://doi.org/10.1109/TPEL.2014.2329059

Li, X., Song, Q., Liu, W., Xu, S., Zhu, Z., & Li, X. (2016). Performance Analysis and Optimization of Circulating Current Control for Modular Multilevel Converter. *IEEE Transactions on Industrial Electronics*, *63*(2), 716–727. https://doi.org/10.1109/TIE.2015.2480748

Liu, X., Huang, J., Sun, Y., Gao, S., & Tong, X. (2019). Passive Control for the MMC-HVDC System Based on the Energy Function. *2019 14th IEEE Conference on Industrial Electronics and Applications (ICIEA)*, 2232–2237. https://doi.org/10.1109/ICIEA.2019.8834318

Liu, Z., & Zhao, J. (2021). Disturbance Interaction Analysis and Suppression Strategy of MMC-HVDC Systems Considering Sub-Module Capacitor Voltage Ripples. *IEEE Transactions on Power Systems*, *36*(1), 235–247. https://doi.org/10.1109/TPWRS.2020.3006234

Lizana, R., Perez, M. A., Arancibia, D., Espinoza, J. R., & Rodriguez, J. (2015). Decoupled Current Model and Control of Modular Multilevel Converters. *IEEE Transactions on Industrial Electronics*, *62*(9), 5382–5392. https://doi.org/10.1109/TIE.2015.2405900

Lyu, J., Yin, J., Zhu, H., & Cai, X. (2023). Impedance Modeling and Stability Analysis of Energy Controlled Modular Multilevel Converter. *IEEE Transactions on Power Delivery*, *38*(3), 1868–1881. https://doi.org/10.1109/TPWRD.2022.3225640

Lyu, Y., Li, C., Hsieh, Y.-H., Lee, F. C., Li, Q., & Xu, R. (2017). Capacitor voltage ripple reduction with state trajectory analysis for modular multilevel converter. *2017 IEEE Applied Power Electronics Conference and Exposition (APEC)*, 1829–1836. https://doi.org/10.1109/APEC.2017.7930947

Ma, Y., Lin, H., & Wang, Z. (2019). Equivalent Model of Modular Multilevel Converter Considering Capacitor Voltage Ripples. *IEEE Transactions on Power Delivery*, *34*(6), 2182–2193. https://doi.org/10.1109/TPWRD.2019.2915820

Malinowski, M., Gopakumar, K., Rodriguez, J., & Pérez, M. A. (2010). A Survey on Cascaded Multilevel Inverters. *IEEE Transactions on Industrial Electronics*, *57*(7), 2197–2206. https://doi.org/10.1109/TIE.2009.2030767

Moon, J-W, Kim, C-S., Park, J-W., Kang,D-W., Kim, J-M., (2013). Circulating Current Control in MMC Under the Unbalanced Voltage. *IEEE Transactions on Power Delivery*, *28*(3), 1952–1959. https://doi.org/10.1109/TPWRD.2013.2264496

Nguyen, M. H., & Kwak, S. (2020). Nearest-Level Control Method With Improved Output Quality for Modular Multilevel Converters. *IEEE Access*, *8*, 110237–110250. https://doi.org/10.1109/ACCESS.2020.3001587

Nguyen, M. H., & Kwak, S. (2021). Predictive Nearest-Level Control Algorithm for Modular Multilevel Converters With Reduced Harmonic Distortion. *IEEE Access*, *9*, 4769–4783. https://doi.org/10.1109/ACCESS.2020.3048156

Perez, M. A., Bernet, S., Rodriguez, J., Kouro, S., & Lizana, R. (2015). Circuit Topologies, Modeling, Control Schemes, and Applications of Modular Multilevel Converters. *IEEE Transactions on Power Electronics*, *30*(1), 4–17. https://doi.org/10.1109/TPEL.2014.2310127

Picas, R., Pou, J., Ceballos, S., Zaragoza, J., Konstantinou, G., & Agelidis, V. G. (2013). Optimal injection of harmonics in circulating currents of modular multilevel converters for capacitor voltage ripple minimization. *2013 IEEE ECCE Asia Downunder*, 318–324. https://doi.org/10.1109/ECCE-Asia.2013.6579115

Pou, J., Ceballos, S., Konstantinou, G., Agelidis, V. G., Picas, R., & Zaragoza, J. (2015). Circulating Current Injection Methods Based on Instantaneous Information for the Modular Multilevel Converter. *IEEE Transactions on Industrial Electronics*, *62*(2), 777–788. https://doi.org/10.1109/TIE.2014.2336608

Raza, M., Aslam, A., & Aamir, T. (2023). Performance Analysis of Half-Bridge Commutation Cells of a Modular Multilevel Voltage Source Converter. *IEEC 2023*, 32. https://doi.org/10.3390/engproc2023046032

Reddy, G. A., & Shukla, A. (2019). Arm current sensor-less control of MMC for Circulating current suppression. *2019 IEEE Energy Conversion Congress and Exposition (ECCE)*, 6905–6910. https://doi.org/10.1109/ECCE.2019.8913028

Reddy, G. A., & Shukla, A. (2021). Circulating Current Optimization Control of MMC. *IEEE Transactions on Industrial Electronics*, *68*(4), 2798–2811. https://doi.org/10.1109/TIE.2020.2977565

Ren, J., Li, W., & Zhang, S. (2021). Study on AC Harmonic Characteristics of Netherland ±525kV/2GW MMC-HVDC System for Offshore Wind Farms Integration. *2021 International Conference on Power System Technology (POWERCON)*, 1534–1541. https://doi.org/10.1109/POWERCON53785.2021.9697553

Ronanki, D., & Williamson, S. S. (2018). Modular Multilevel Converters for Transportation Electrification: Challenges and Opportunities. *IEEE Transactions on Transportation Electrification*, *4*(2), 399–407. https://doi.org/10.1109/TTE.2018.2792330

Sang, Y., Yang, B., Shu, H., An, N., Zeng, F., & Yu, T. (2019). Passive Current Control Design for MMC in HVDC Systems through Energy Reshaping. *Electronics*, *8*(9), 967. https://doi.org/10.3390/electronics8090967

Song, Q., Liu, W., Li, X., Rao, H., Xu, S., & Li, L. (2013). A steady-state analysis method for a modular multilevel converter. *IEEE Transactions on Power Electronics*, *28*(8), 3702–3713. https://doi.org/10.1109/TPEL.2012.2227818

Spier, D. W., Prieto-Araujo, E., Gomis-Bellmunt, O., & Mestre, J. L. (2021). Analytic estimation of the MMC sub-module capacitor voltage ripple for balanced and unbalanced AC grid conditions. https://doi.org/10.48550/arXiv.2109.00310

Thakur, S., Odavic, M., Allu, A., Zhu, Z. Q., & Atallah, K. (2022a). Analytical Modelling and Optimization of Output Voltage Harmonic Spectra of Full-Bridge Modular Multilevel Converters in Boost Mode. *IEEE Transactions on Power Electronics*, *37*(3), 3403–3420. https://doi.org/10.1109/TPEL.2021.3108877

Thakur, S., Odavic, M., Allu, A., Zhu, Z. Q., & Atallah, K. (2022b). Analytical Modelling and Optimization of Output Voltage Harmonic Spectra of Full-Bridge Modular Multilevel Converters in Boost Mode. *IEEE Transactions on Power Electronics*, *37*(3), 3403–3420. https://doi.org/10.1109/TPEL.2021.3108877

Tu, Q., & Xu, Z. (2011). Impact of sampling frequency on harmonic distortion for modular multilevel converter. *IEEE Transactions on Power Delivery*, *26*(1), 298–306. https://doi.org/10.1109/TPWRD.2010.2078837

Tu, Q., Xu, Z., Huang, H., & Zhang, J. (2010a). Parameter design principle of the arm inductor in modular multilevel converter based HVDC. *2010 International Conference on Power System Technology: Technological Innovations Making Power Grid Smarter, POWERCON2010*, 0–5. https://doi.org/10.1109/POWERCON.2010.5666416

Tu, Q., Xu, Z., Huang, H., & Zhang, J. (2010b). Parameter design principle of the arm inductor in modular multilevel converter based HVDC. *2010 International Conference on Power System Technology: Technological Innovations Making Power Grid Smarter, POWERCON2010*, 0–5. https://doi.org/10.1109/POWERCON.2010.5666416

Uddin, W., Hussain, S., Zeb, K., Khalil, I. U., Ullah, Z., Dildar, M. A., Adil, M., Ishfaq, M., Khan, I., & Kim, H. J. (2018). Effect of Arm Inductor on Harmonic Reduction in Modular Multilevel Converter. *2018 International Conference on Power Generation Systems and Renewable Energy Technologies (PGSRET)*, 1–5. https://doi.org/10.1109/PGSRET.2018.8685973

Vasiladiotis, M., Cherix, N., & Rufer, A. (2014). Accurate Capacitor Voltage Ripple Estimation and Current Control Considerations for Grid-Connected Modular Multilevel Converters. *IEEE Transactions on Power Electronics*, *29*(9), 4568–4579. https://doi.org/10.1109/TPEL.2013.2286293

Wang, Y., Huang, Z., Yuan, Y., Gao, L., & Li, P. (2016). Harmonics analysis and simulation of NLM in MMC. *12th IET International Conference on AC and DC Power Transmission (ACDC 2016)*, 3 (6 .)-3 (6 .). https://doi.org/10.1049/cp.2016.0383

Xi, Q., Tian, Y., & Fan, Y. (2024). Capacitor Voltage Balancing Control of MMC Sub-Module Based on Neural Network Prediction. *Electronics*, *13*(4), 795. https://doi.org/10.3390/electronics13040795

Xiao, H., Xu, Z., Xue, Y., & Tang, G. (2013). Theoretical analysis of the harmonic characteristics of modular multilevel converters. *Science China Technological Sciences*, *56*(11), 2762–2770. https://doi.org/10.1007/s11431-013-5331-1

Xu, C., Lin, L., Yin, T., & Hu, J. (2020). An Improved Phase-Shifted-Carrier Technique for Hybrid Modular Multilevel Converter with Boosted Modulation Index. *IEEE Transactions on Power Electronics*, *35*(2), 1340–1352. https://doi.org/10.1109/TPEL.2019.2921202

Xu, Z., Xiao, H., & Zhang, Z. (2016). Selection methods of main circuit parameters for modular multilevel converters. *IET Renewable Power Generation*, *10*(6), 788–797. https://doi.org/10.1049/iet-rpg.2015.0434

Yuan, Y., Li, P., Kong, X., Liu, J., Li, Q., & Wang, Y. (2016). Harmonic influence analysis of unified power flow controller based on modular multilevel converter. *Journal of Modern Power Systems and Clean Energy*, *4*(1), 10–18. https://doi.org/10.1007/s40565-015-0175-2

Yuvaraja, T., & Mazumder, S. (n.d.). Performance and Analysis of Modular Multilevel Converter. *American Journal of Engineering Research*, 2014. https://www.ajer.org

Zhang, B., & Nademi, H. (2020). Modeling and Harmonic Stability of MMC-HVDC With Passive Circulating Current Filters. *IEEE Access*, *8*, 129372–129386. https://doi.org/10.1109/ACCESS.2020.3009331

Zhang, H., Belhaouane, M. M., Colas, F., Kadri, R., Gruson, F., & Guillaud, X. (2021). On Comprehensive Description and Analysis of MMC Control Design: Simulation and Experimental Study. *IEEE Transactions on Power Delivery*, *36*(1), 244–253. https://doi.org/10.1109/TPWRD.2020.2977470